Tectonophysics 807 (2021) 228813

Contents lists available at ScienceDirect

Tectonophysics

journal homepage: www.elsevier.com/locate/tecto

Deep-sea submarine erosion by the Kuroshio Current in the Manila accretionary prism, offshore Southern Taiwan

Prabodha Das [a], Andrew Tien-Shun Lin [a,*], Min-Pen Philip Chen [b], Elda Miramontes [c,d], Char-Shine Liu [e], Neng-Wei Huang [f], Jennifer Kung [g], Shu-Kun Hsu [a], Radha Krishna Pillutla [a,h], Kalyani Nayak [a,h]

[a] Department of Earth Sciences, National Central University, Zhongli Dist., Taoyuan City 32001, Taiwan
[b] Institute of Oceanography, National Taiwan University, Taipei City 10617, Taiwan
[c] Faculty of Geosciences, University of Bremen, Bremen 28359, Germany
[d] MARUM – Center for Marine and Environmental Sciences, University of Bremen, Bremen 28359, Germany
[e] Ocean Center, National Taiwan University, Da'an District, Taipei City 10617, Taiwan
[f] Sinotech Engineering Consultants, Ltd., Sungshan Dist., Taipei City 105052, Taiwan
[g] Department of Earth Sciences, National Cheng-Kung University, Tainan City 70101, Taiwan
[h] Earth System Science Program, Taiwan International Graduate Program, Academia Sinica and National Central University, Taiwan

ARTICLE INFO

Keywords:
Taiwan
Manila subduction zone
Kuroshio current
Luzon strait
Bottom currents

ABSTRACT

The Kenting Plateau is characterized by unusual low relief surfaces that straddle the topographic crest of the northern Manila accretionary prism off southern Taiwan at 400–700 m water depth. Multibeam bathymetric data, reflection seismic data, Acoustic Doppler Current Profiler (ADCP) data, surface grab samples, and sediment cores were collected in and around the Plateau to identify evidence of erosion in the Kenting Plateau and understand how the morphological evolution has been influenced by submarine erosion over geological time scales. The most distinctive feature on the Kenting Plateau is a 3 km × 7 km bean-shaped flat elevated platform (Kuroshio Knoll) revealed by multibeam bathymetry. Seismic data show almost no reflections beneath the seafloor and erosional truncations at the seafloor, especially in the Plateau's eastern half, evidencing widespread erosion. The P-wave velocity of the gravels recovered from the top of the Plateau ranges from 2.2 to 4 km/s. After comparing the velocity with the borehole data from nearby basin the burial depth of the parent rocks was found to be around 2 to 4 km below the seafloor, indicating that the parent rocks have been uplifted and gravels were formed due to erosion of the Plateau. The truncation of the seafloor shown on seismic sections suggests significant erosion on the Plateau. Sand content of the sediment cores decreases away from the Plateau, suggesting that sediment transport is effective in this area with high energy deposition, thereby accumulating coarse sediments on the Plateau and removing fine particles away from it. The presence of a dune field migrating northward of the Plateau, parallel to the Kuroshio Current also evidences active sediment transport in the area. Flow velocity of the Kuroshio Current observed from the ADCP data is very high, reaching up to 1.8 m/s on top of the Kuroshio Knoll (SE domain). We thus interpret that the observed intense erosion is caused by the Kuroshio Current, while the uplift of the Kenting Plateau is partially due to isostatic rebound caused by sediment removal through erosion and compression of the accretionary wedge. The higher sedimentation rate and coarser in grain size during sea level lowstand (20,000–12,000 yrs. BP) suggests that the erosion was more intense during the glacial period compared to that of deglacial period (< 12,000 yrs. BP) as seen from the MD97–2145 core. Submarine erosion is predominant throughout the Plateau, and it controls the geomorphology of the Plateau, especially the Kuroshio Knoll.

* Corresponding author.
E-mail address: andrewl@ncu.edu.tw (A.T.-S. Lin).

https://doi.org/10.1016/j.tecto.2021.228813
Received 6 January 2021; Received in revised form 27 February 2021; Accepted 2 March 2021
Available online 5 March 2021

1. Introduction

The processes controlling the geomorphological evolution of terrestrial landscapes are relatively well-known. Precipitation and tectonic uplift are the two main factors driving erosion in a mountainous topography (Montgomery and Greenberg, 2000). On the contrary, the principal factors controlling the submarine erosion are poorly understood, primarily due to the paucity of repeated surveys over an area to monitor its evolution.

Ocean currents play an essential role in shaping the seafloor by generating submarine erosion, controlling sediment transport and deposition in the shallow and deep-marine environment (Rebesco et al., 2014; Miramontes et al., 2019a; Zhao et al., 2019). There have been many studies about submarine erosion of the bedrock in volcanoes, seamounts, guyots, or submarine canyons, where erosion is mainly caused by gravitational processes, including slope failure and gravity flows (Mitchell et al., 2003; Romagnoli et al., 2012; Mitchell, 2014; Watson et al., 2017). Although the erosion of sediments due to bottom currents that results in the formation of features such as contourite channels, furrows, scours and bedforms has been already documented in several areas on the ocean floor (Rebesco et al., 2014; García et al., 2016; Hernández-Molina et al., 2017; Miramontes et al., 2019a), it is to date not clear whether the oceanic circulation can play an essential role on the erosion of consolidated and lithified substrate and thus whether they contribute to the erosion of the top of submarine plateaus, ridges, and seamounts.

The Kenting Plateau, located south of Taiwan, is an example of a flat-topped plateau of unclear origin. Conventional interpretation envisions that the plateau uplift and erosion is mainly governed by structural and tectonic processes related to the Manila subduction zone, which can cause significant slope failure or mass wasting of the Plateau (Lin et al., 2008; Lester et al., 2013). However, previous interpretations never considered the role of oceanographic processes in the erosion of the Kenting Plateau. Considering that the Plateau is also subjected to the permanent impact of the Kuroshio Current (Jan et al., 2015; Nan et al., 2015), we hypothesize that the Kuroshio Current may erode the top of the Plateau. In this study, we aim to investigate the ongoing erosional processes on the Kenting Plateau. We performed combined analyses of multibeam bathymetry, seismic reflection data, P-wave velocity data of gravels, sediment cores along with current velocity measurements with the specific aims of: (i) identifying fine-scale and broad geomorphic features in the Kenting Plateau seafloor to understand different processes acting upon the Plateau; (ii) characterizing the sediment composition and distribution in the study area; (iii) identifying evidence of erosion in the Kenting Plateau; and (iv) discussing how submarine erosion shaped the morphology of the Kenting Plateau over geological time scales.

2. Physical setting

2.1. Geological setting

Taiwan is located in the active orogenic belt formed by the collision of the Eurasian plate with the overriding Luzon volcanic arc (Fig. 1). Marine geophysical investigations suggested that the active submarine Taiwan orogen is doubly vergent, with active west-vergent thrust faults along the frontal slope (western) facing the Manila trench, and east-directed backthrusts along the rear arcward slope (eastward) of the accretionary prism (Liu et al., 1992; Reed et al., 1992). The submarine Kenting Plateau is located in the upper accretionary wedge and the hangingwall of a splay fault, or out-of-sequence thrust, off southern Taiwan (Fig. 1; Reed et al., 1992; Lin et al., 2009). Around 50 km off the Hengchun peninsula, the upper accretionary wedge becomes a wide and shallow submarine plateau of unusual bathymetry characterized by low relief with subdued hills and broad valleys. This large submarine plateau is elevated above the more rugged bathymetry that characterizes the rest

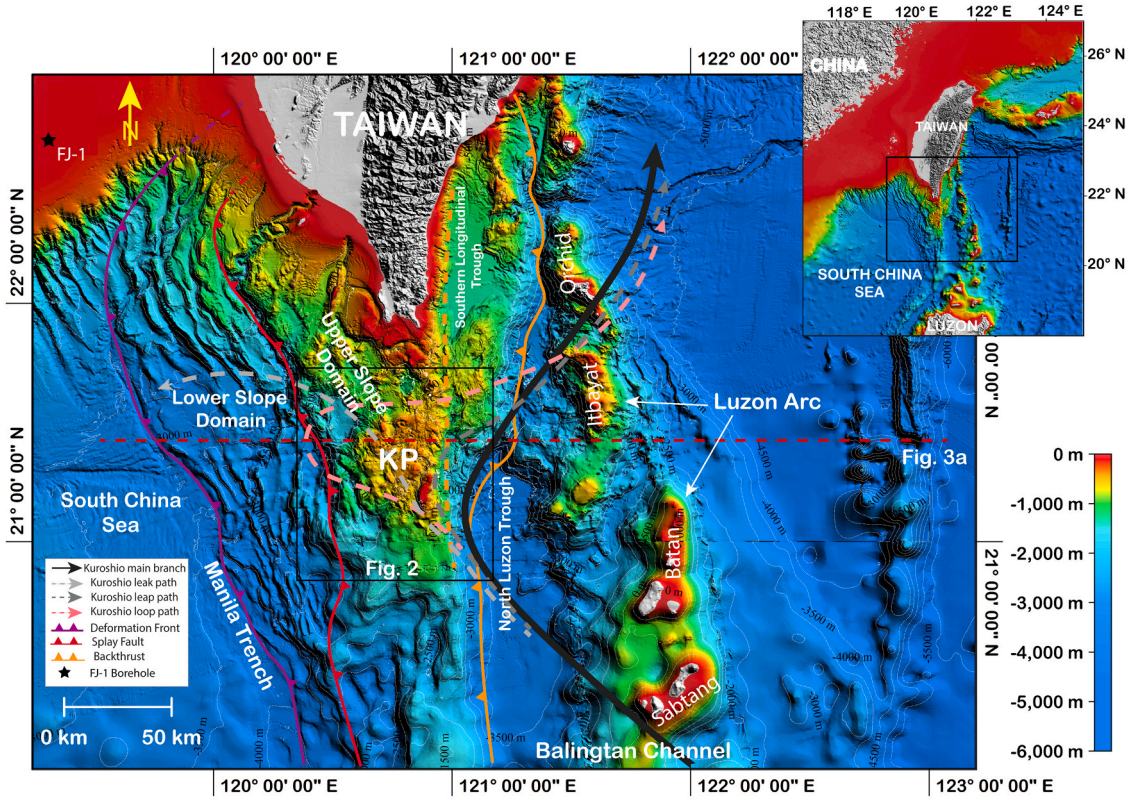

Fig. 1. Bathymetric map around offshore southern Taiwan, showing the major geological structures and tectonic provinces, including the northern Manila subduction zone and the Luzon volcanic arc. 'KP' indicates Kenting Plateau. Rectangle in the map indicates the location of Fig. 2.

of the submarine accretionary wedge, and it lies at around 400–700 m water depth and has an area of 1200 km^2 (Fig. 1).

The Kenting Plateau, a kidney-shaped uplifted area, lies north in the upper accretionary wedge of the Manila subduction zone (Figs. 1, 2). The northern side of the Kenting Plateau is bounded by a topographic low, which separates it from the Taiwan Island (Fig. 1). The Plateau is restricted to the upper slope of the Manila accretionary prism, which is not connected to the main Taiwan island by any submarine canyons or channels for sediment transport and dispersal. The Plateau is nearly ~50 km away from Taiwan's main landmass and between the Plateau and Taiwan there is a ~ 1000 m deep and ~ 10 km wide trough (Fig. 2). The eastern side of the Kenting Plateau is separated from the Luzon volcanic arc by a deep trough called North Luzon Trough, and the southern part, by a deeper upper accretionary wedge down to 1500–2000 m deep (Fig. 1). The Luzon Strait encompasses the area between Taiwan and Luzon Islands. The strait is about 360 km wide and consists of few narrow passages separated by many small islands. Therefore, the bathymetry is varying from very shallow water depth in the accretionary wedge and the volcanic arc terrains to deep marine in the Luzon forearc basin (down to 3800 m deep). The western side of the Plateau is comprised of several elongated ridges with slope basins (e.g. Dirgantara et al., 2020). The bathymetry of the upper accretionary wedge shows a gradually shallowing trend towards the rear wedge and near the North Luzon Trough, from around 1500 m in the west to around a few hundred meters along the summit of the rear wedge. In the SE domain of the Plateau, there is an elevated area having water depths of less than 100 m (herein named, Kuroshio Knoll, for the first time; Fig. 2). The Plateau is surrounded by a few perched basins, the largest one (Kenting Basin, named for the first time) on the north-western side, and the second largest (Hobi Basin, named for the first time) on the south-western side of the Plateau (Fig. 2).

2.2. Oceanographic setting

The Kuroshio Current is the westernmost current of the North Pacific subtropical gyre that emerges from the North Equatorial Current (NEC) (Nitani, 1972; Qiu and Lukas, 1996). After flowing along the east coast of the Philippines, the NEC bisects into two branches, the south-bound Mindanao Current and the north-bound Kuroshio Current (Nitani, 1972; Qiu and Lukas, 1996; Qu and Lukas, 2003; Zhai and Hu, 2013). The diameter of the Kuroshio Current, defined by meridional velocity $v \geq 0.2$ m/s, varies from 85 to 135 km, and the thickness oscillates between 400 and 600 m (Jan et al., 2015). The observed maximum velocity, according to Jan et al. (2015), located at 23.750 N, varies between 0.7 and 1.4 m/s. The Kuroshio Current splits during its course from the east coast of the Philippines northward to Japan. A part of the Kuroshio Current flows into the South China Sea through the Balintang Channel (Fig. 1; Chern and Wang, 1998; Liang et al., 2008). This branch of the Kuroshio Current is called Kuroshio Intrusion (KI) (Fig. 1). The KI occurs in the vicinity of the Kenting Plateau. This infiltration impacts the dynamic cycles in the South China Sea, influencing the temperature, salinity, and flow circulation in the northeastern South China Sea (Li et al., 1998; Wu and Chiang, 2007; Xiu et al., 2010; Nan et al., 2011; Wu, 2013). The different infiltration paths vary from a direct branch (Qiu, 1984), a Loop Current (Li and Wu, 1989), and anticyclonic rings (Li et al., 1998). The KI displays a seasonal variability, being more intense in winter than in summer (Wyrtki, 1961; Shaw, 1991). The surface water carried by the Kuroshio Current can barge profoundly into the South China Sea, particularly in winter (Centurioni et al., 2004).

Equatorial and tropical planktonic diatoms have been used as a proxy to reconstruct the Kuroshio Current's long-term fluctuation (Jiang et al., 2006). Major warm periods coincide with a relatively strong impact of the Kuroshio Current in the South China Sea. The strongest intrusion of Kuroshio Current occurred during most of the Holocene and the very late phase of MIS 5e (Jiang et al., 2006).

3. Materials and methods

3.1. Bathymetric data for seafloor characterization

In this study, we use multibeam bathymetry collected during three cruises. Multibeam bathymetric data were acquired aboard the R/V MV AODIS and the R/V POLARIS in 2017 using a 30 kHz Kongsberg EM302 multibeam echo sounder. The entire survey encompassed 6197 km^2 in

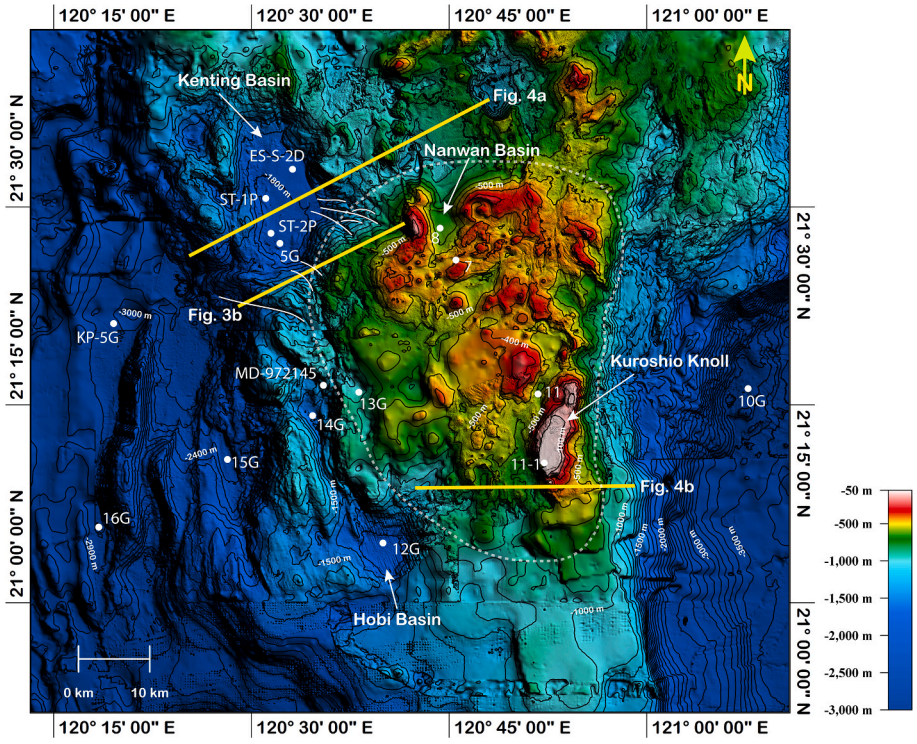

Fig. 2. Shaded relief map with contours every 100 m in and around the Kenting Plateau, showing the location of basins and the location of sediment cores (white circles) and selected seismic lines (yellow lines). The site 11–1 is the location of algae and other living organisms collected on the Plateau. The transparent dashed white line suggests rough boundary of the Kenting Plateau. The solid white lines indicate the location of erosive gullies and the pathways for transporting sediments from the top of the Plateau to the basins. See Fig. 1 for location. (For interpretation of the references to colour in this figure legend, the reader is referred to the web version of this article.)

the Kenting Plateau, especially the northern part and its surrounding area. The multibeam bathymetry data of the south-eastern part of the Plateau were collected in 2018 using the multibeam echo sounder Atlas MD50 system operated at a frequency of 50 kHz onboard R/V Ocean Researcher II. The average water depth for the 3500 km^2 region across the Plateau is ~600 m and within a range of 68 to 1500 m, water depths adapted for the EM302 and Atlas MD50 multibeam echosounder systems. All the data were post-processed and displayed with the CARAIBES and GMT software, respectively.

3.2. Seismic reflection data for seafloor and sub-seafloor characterization

2D multichannel reflection seismic data sets collected during the oceanographic cruises R/V Ocean Researcher I (OR1)-1046, R/V OR1-1083b, and R/V Marcus G. Langseth were used in this study to distinguish between different geomorphic features on the Plateau. MGL0905–23 (Fig. 3a) and MGL0905–27 (Fig. 4a) data were collected during the summer of 2009 through the project TAIGER (Taiwan Integrated Geodynamics Research), a joint research program between the USA and Taiwan. Research vessel R/V Marcus G. Langseth with a source array of 36 air guns and a total volume of ~6600 $in.^3$ towed at 8 m water depth was used to collect the data. Shots were dispersed every 50 m and recorded at the same time by a 468 channel, 6 km long. The 2D seismic data MCS-1046 (Fig. 3b) were collected in August 2013 using 108 channels with 12.5 m channel spacing. Shots were discharged at 6 to 10 s spans with a nominal shot interval of 12.5 m. The 2D seismic data MCS-1083b (Fig. 4b) were collected in July 2014. An air-gun array, consisting of three air guns with a total compressed air volume of 950 $in.^3$, was towed behind the R/V OR1 and fired at a 12 s interval, using 108 channels, 12.5 m channel spacing. The seismic data were processed in the Institute of Oceanography, National Taiwan University (IONTU), Taiwan.

3.3. Sediment cores and grab samples

Three piston cores and nine gravity cores are used in this study, which were retrieved during the OR1–930 (June 2010) and OR1–1138 (June 2016), OR1–1029 (March 2013), OR5–0032 (February 2016), and MD1997 cruises (Fig. 2). Sediment cores were split into two halves lengthwise, photographed, and visually described. The cores were sampled every 1 cm except for MD97–2145. The core MD97–2145 was processed for grain size analysis in IONTU, Taiwan. The grain size of core MD97–2145 was measured every centimeter in the 0–40 cm interval, every 10 cm between 40 and 430 cm, and every 5 cm from 430 to 2355 cm. Grain size analysis of sediments was carried out using a Beckman Coulter LS 13320 particle size analyzer. All samples were washed with distilled water and hydrogen peroxide to remove salt and organic materials, respectively, then treated with hydrogen chloride to remove carbonate. Afterward, the samples were treated with sodium hexametaphosphate $(NaPO_3)_6$ for particle dispersion. The results were

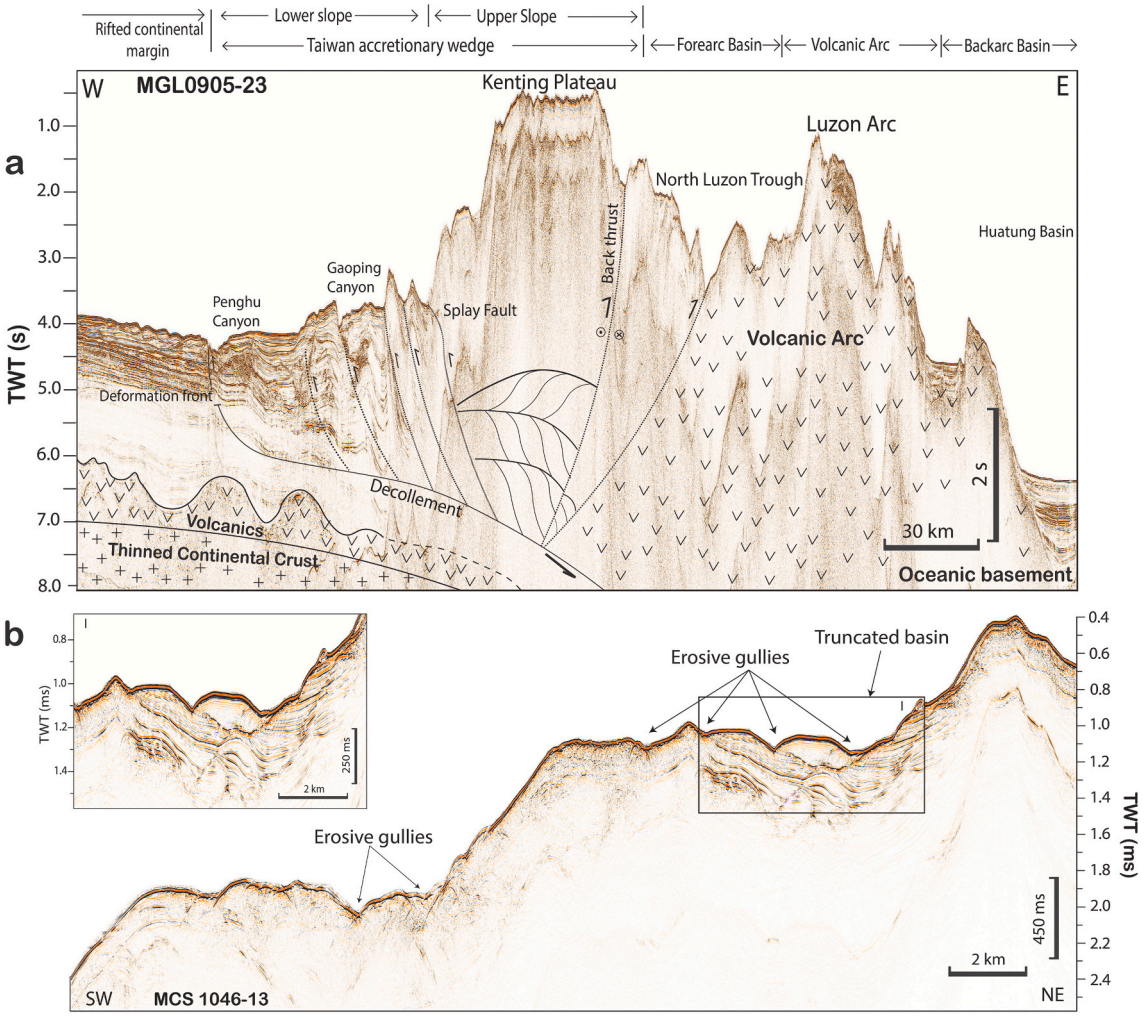

Fig. 3. a) Seismic line MGL0905–23 passing through the Kenting Plateau, showing tectonic setting of the study area (See Fig. 1 for profile location). b) Seismic lines of MCS1046–13 showing erosive gullies and truncated basin in the northwestern part of the Plateau near the Kenting Basin. See Fig. 2 for the location of 3b.

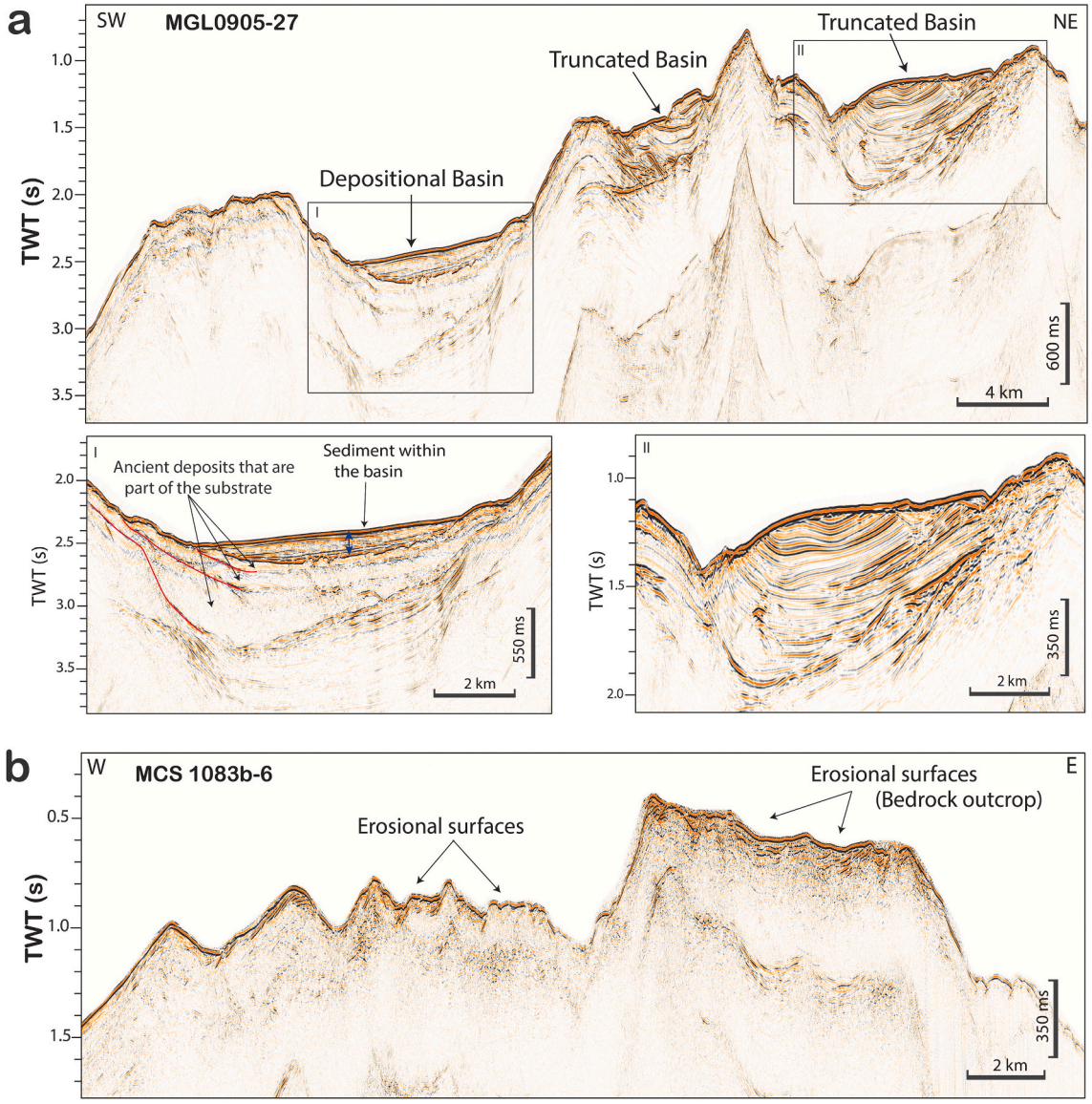

Fig. 4. a) Seismic line MGL0905–27 showing a depositional basin (Kenting Basin) and a truncated basin in the northwestern part of the Plateau. b) Seismic lines of MCS1083b-6 showing bedrock outcropping at the seafloor and erosional surfaces at the southern extension of the Kuroshio Knoll across the southern tip of the Kenting Plateau. See Fig. 2 for the location.

calculated and plotted using the software GRADISTAT (Blott and Pye, 2001) and SIGMAPLOT, respectively. For core MD97–2145, grain size distribution within the grain size range of 0.16 to 1000 μm was recorded by a laser particle size analyzer, and particles coarser than 1000 μm were measured by sieving.

During the cruise OR1–1138 in June 2016, seafloor grab-samples containing gravels were recovered within the Plateau (Fig. 5). P-wave velocity was measured in these gravels. For measuring the P-wave velocity, the gravels were dried overnight, and the end surfaces of the gravels were polished on both sides to give an adequate coupling between the transducer surface and the gravel surface to expand the exactness of the travel time estimation. Stiffer grease was utilized as a coupling specialist in this investigation. Transducers were squeezed to each surface of the gravel, and the transit time was noted. The P-wave speed was determined by separating the length of the rock test by the transit time. The tests were redone at least twice for all different diameter samples, and the average value was considered the P-wave velocity value (Fener, 2011).

3.4. Radiocarbon dating and age reconstruction

We employed the age determination and sedimentation rate of the core MD97–2145 from Huang (2002). Fifteen samples of planktonic foraminifera were picked from the core MD 97–2145 in IONTU, Taiwan, and were dated using accelerator mass spectrometry (AMS) ^{14}C at the Rafter Radiocarbon Laboratory in New Zealand for the age reconstruction. The dated ages were further calibrated for the sedimentation rate.

3.5. Current velocity data

In this study, we used a Vessel-Mounted Acoustic Doppler Current Profiler (VM-ADCP) Ocean Surveyor 150 kHz acquired during the oceanographic cruise R/V OR2 conducted during 18th September to 22nd September 2018. This system measures current velocities down to about 200 m below sea level. The ADCP data were post-processed with the software CASCADE V7.2.

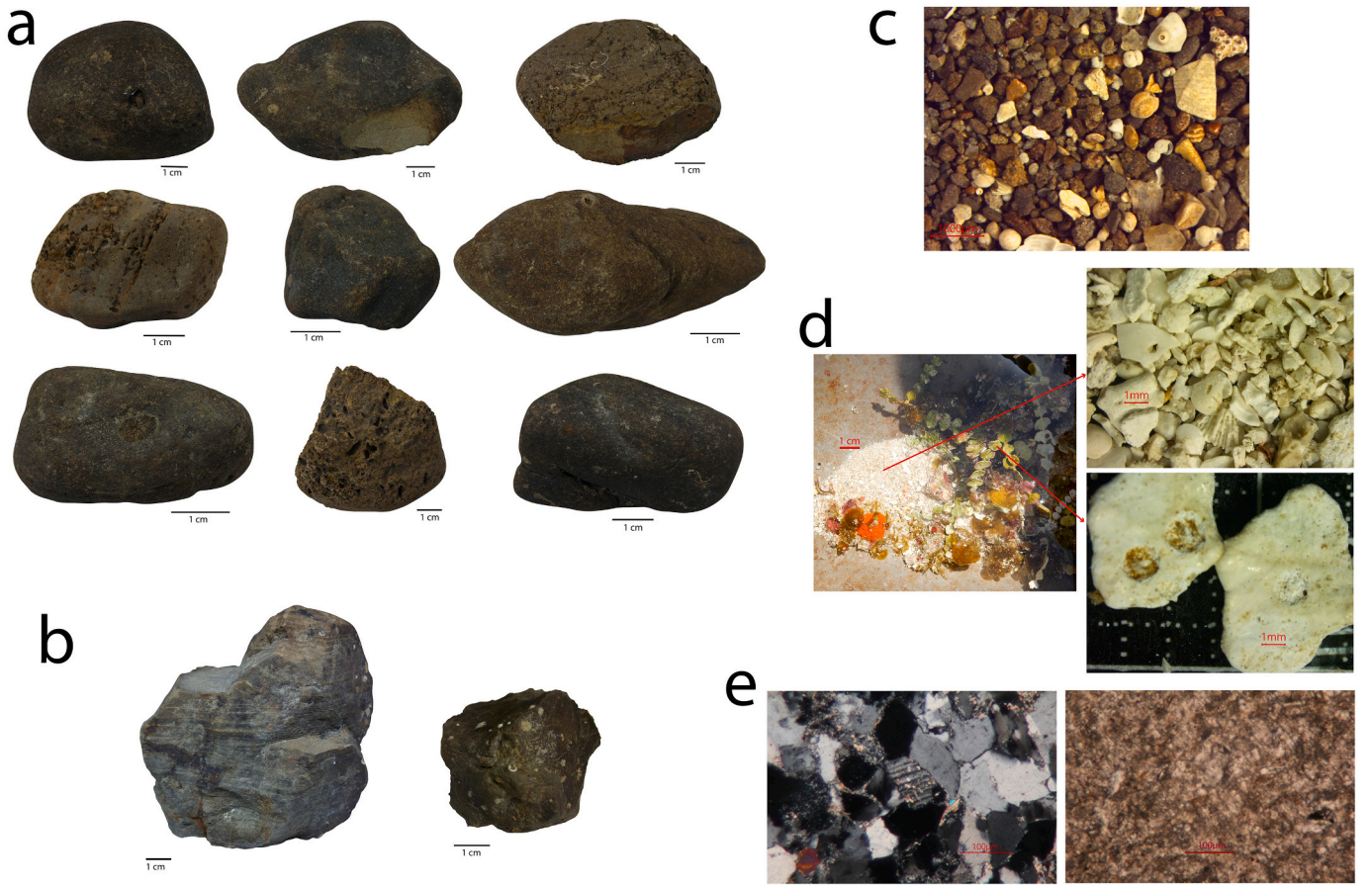

Fig. 5. a) Gravels recovered from site OR-1-1138-11. Each bar is 1 cm. b) Gravels recovered from site OR-1-1138-7. Each bar is 1 cm. c) Stereoscopic image of broken fragments of shells, foraminifera and sand collected from site OR-1-1138-8. d) Carbonate samples and living algae collected from the Kuroshio Knoll at site OR1–1138-11-1. e) Thin sections of the gravels from site OR-1-1138-11.

4. Results

4.1. Submarine geomorphology of the Kenting Plateau

The features identified on the multibeam bathymetry and seismic reflection datasets allowed detailed mapping of the Kenting Plateau. The geomorphological and geological features in and around the Kenting Plateau were divided into depositional basins, truncated sedimentary basins, bedrock outcrops, bedform fields, and the Kuroshio Knoll, an unusual flat topped bathymetric high, respectively.

4.1.1. Depositional basins

These are geomorphological depressions with stratified reflections immediately beneath the seafloor that are conformable to the seafloor reflections, indicating active depositional features. There are a few small basins identified on the Plateau surface, with the largest one named the "Nanwan Basin", for the first time, having an area of ~36 km^2 (Fig. 2). Other basins on top of the Plateau surface are relatively small depressions by size. There are two larger basins by the area outside of the Plateau. Kenting Basin, located in the northwest of the Plateau, is the largest basin around ~126 km^2 in area (Fig. 2). Another basin named "Hobi Basin" lies to the Plateau's southwest with an area around ~39 km^2 (Fig. 2). The basin consists of pelagic sedimentary deposits that are stratified, parallel reflections of low to moderate amplitude with little thickness variation oscillates between 2.450 and 2.650 s two-way travel time (TWT), and around ~300 m thickness (Fig. 4a). These thick sediment piles overlie unconformably on older sediments that are part of the substrate (mass transported deposits) characterized by chaotic and transparent reflections (Fig. 4a).

4.1.2. Truncated sedimentary basins

Truncated basins are areas where stratal reflections are truncated on the seafloor, indicating the seafloor's erosive nature. Truncated basins occur mainly in the northwest and west sides of the plateau (Figs. 3b, 4a). These basins record some degree of deformation. They are folded and titled by tectonic processes.

4.1.3. Bedrock outcrops

Bedrock outcrops are characterized by rough bathymetry, localized steep gradients, and chaotic seismic reflections beneath the seafloor. In some places, truncations can also be identified. Bedrock outcrops are mainly located in the eastern half of the Kenting Plateau near the boundary with the forearc basin (Fig. 4b). A grab sample recovered corals and a few benthic organisms that live on rigid substrates on the southern part of elevated flat top surface, Kuroshio Knoll (Fig. 5d). Bedrock outcrops, including the top surface of the elevated Knoll, are interpreted to be erosive surfaces that can be sporadically overlain in some bathymetric lows by a thin layer of recent coarse-grained materials. Gravels and sands were recovered at some sites (e.g., at sites OR1–1138-7 and OR1–1138-11; Fig. 5).

4.1.4. Bedform fields

The presence of regularly spaced asymmetric crescent-shaped bedforms are well identified in the multibeam bathymetry (Fig. 6, Profile A-A′ and B-B′) in the Nanwan Basin located on the north side of the Plateau (Fig. 2). The basin is surrounded by structural highs (Fig. 6) and deepens from south to north from ~550 m to ~900 m. These are parallel crescent-shaped bedforms pointing northward and having a height of ~5 m, wavelength ranges between 130 m to 180 m, and stretched over

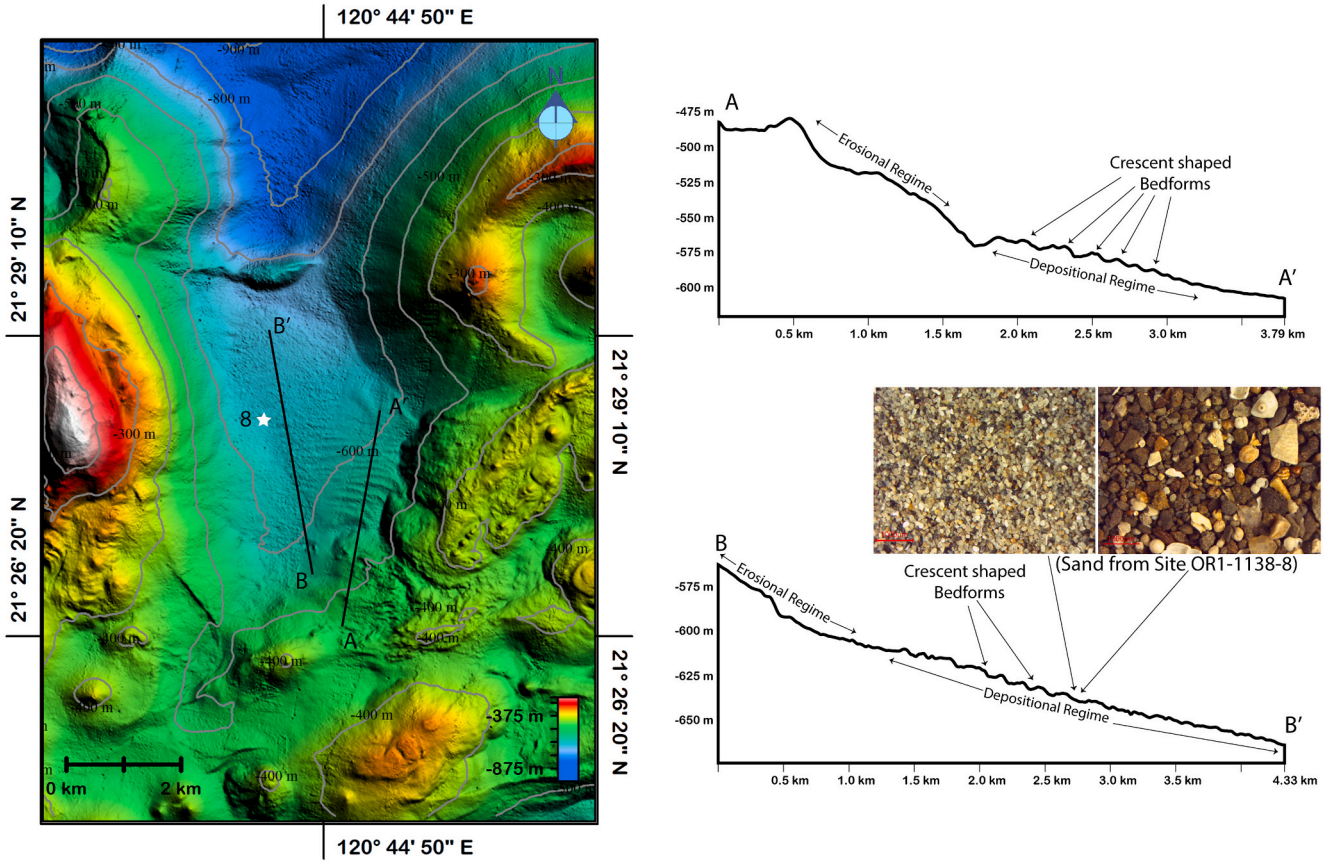

Fig. 6. Multibeam bathymetry of the Nanwan Basin in the northern part of the Plateau. The white star indicates the location of site OR1–1138-8. Two different topographic profiles A-A′, B-B′ show the presence of crescent shaped bedforms (dunes) on the basin floor, and images of the sandy sediments collected at site OR-1-1138-8.

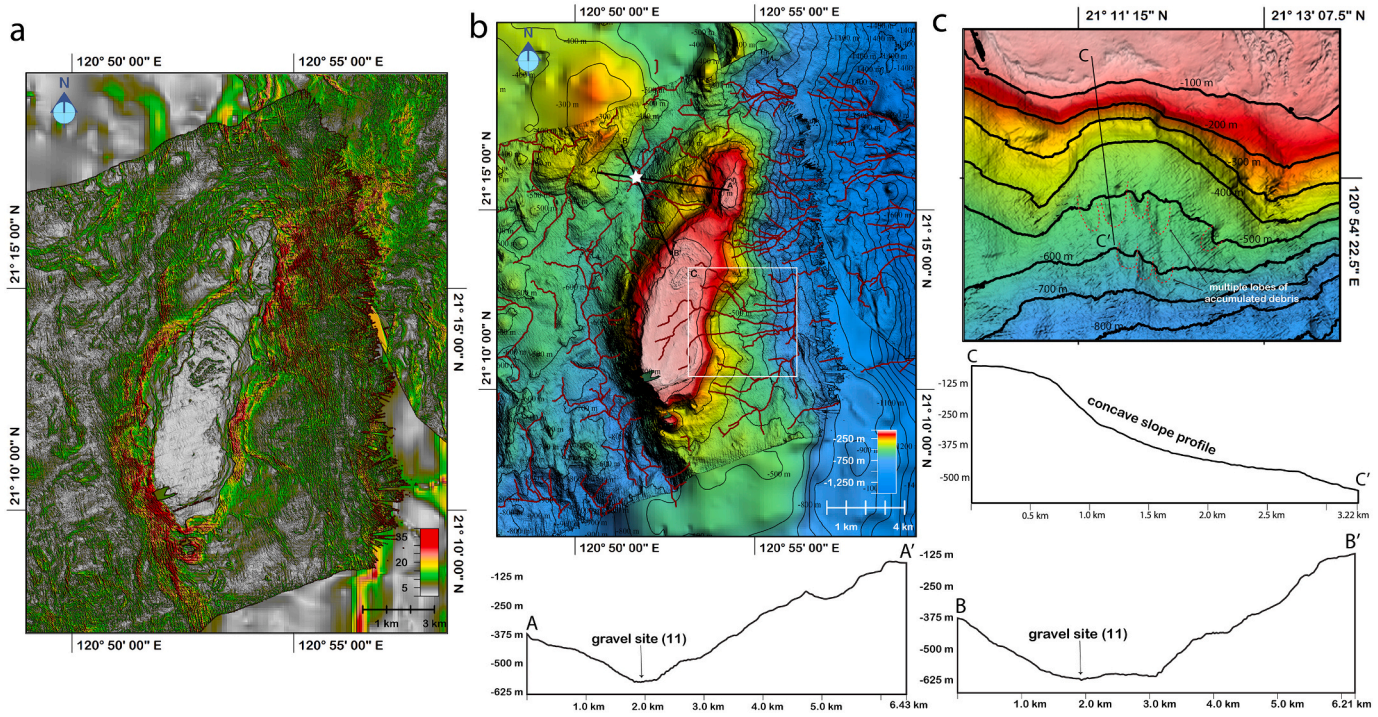

Fig. 7. a) Slope profile of the Kuroshio Knoll and surrounding area. b) Drainage map of the Kuroshio Knoll and adjacent area. The profile A-A′ and B-B′ show the profile passing through the gravel location OR1–1138-11. c) Slope failure debris identified as multiple lobes of accumulated debris.

~1400 m in crest length from east to west. These bedforms lie on the seafloor with a slope of 1 ° – 7 ° and a water depth of ~550 m to ~700 m (Fig. 6, Profile A-A′ and B-B′). The sediment accumulated in this basin is fine to coarse sands with abundant broken shell fragments. The grain size varies between 0.2 mm and more than 1 mm (Fig. 6).

4.1.5. The Kuroshio Knoll

The most peculiar feature on the Kenting Plateau lies in the southeast region, a 3 km × 7 km bean-shaped flat and elevated platform with a few steep concave scarps on its flank, which is named "Kuroshio Knoll" (Fig. 2). The Kuroshio Knoll's flat top lies at a depth of around ~70 m, and its base lies at around ~600 m water depth. A narrow channel-like depression surrounds the Knoll in the western part, and in the eastern part, it extends towards the deep ocean. The slope gradient commonly exceeds around ~18°, with the maximum values up to 36° in the scarp area and slowly diminishes below 500 m water depth (Fig. 7a). The eastern flank of the Knoll has a concave shape related to slope failure. The debris is transported from the Knoll to the deep sea by mass-wasting processes, and some debris is accumulated as inferred lobes of sediments (Fig. 7c).

4.2. Sediment characteristics

Coarse gravels of sedimentary rocks along with sands and granules were recovered at Sites OR1–1138-7, OR1–1138-8, and OR1–1138-11 (Figs. 5a, b, c). The gravels are well-lithified sandstones, mudstones, and a few carbonate rocks. The sandstone gravels are well-cemented and consist of angular to sub-angular quartz, rock fragments, and feldspar as observed in thin sections (Fig. 5e). The parent rocks are probably from nearby bathymetric highs defined from reflection seismic data as "hard surfaces" and underlain by basement rocks (Fig. 4b). The basement rocks must have been buried in a certain depth to achieve the state of diagenesis observed in the recovered gravels. The measured P-wave velocities of gravels are compared with the sonic velocity profile (compaction curve) from a nearby borehole (FJ-1) in the Tainan basin, reported by Lin et al. (2003). The compaction curve is commonly used to estimate depths of sediment burials (Issler, 1992; Audet, 1995; Audet, 1996). Our comparison indicates that the parent rocks were buried in a depth ranging from 2.2 to 4.5 km (Fig. 8).

Few large basins surround the Plateau and a few small basins occur within the Plateau, and several sediment cores recovered from most of the basins in and around the Plateau have been analyzed in this study. These basins are well drained from the Kenting Plateau with several gullies/channels (Figs. 2, 3b). The sediment type in those cores collected from the Plateau mainly consists of fine- to medium-grained sands with a few patches of medium to coarse sand layers (Fig. 9). In the Plateau's distal region, the sediment cores are mainly composed of mud (hemipelagic and/or turbiditic mud) with few patches of fine to medium-grained sand layers (Fig. 9). To better understand the sediment transport linked to the oceanic circulation, turbidite deposits were not considered for calculating the volume percentage of sand, silt, and clay of each core. The sediment distribution in those cores shows differences in sand content, decreasing the distance away from the Plateau (Fig. 9). The sand percentage of the core 13G on the Plateau is ~51%, whereas that of the core MD97–2145 located on the western flank of the Plateau is ~20%. The sand content of the cores 5G, STP1, STP2, ES2–2-D from the Kenting Basin lies between ~8 to 15%. The sand content in the sediment core 12G from the Hobi Basin is ~9%. The sand content of the cores KP-5G, 15G, 16G collected from the slope basins far away from the Plateau in the westward direction is between ~1 to 3%. The sand content of 10G in the north Luzon trough is about ~5%. The sand content of the core 14G located in a submarine channel within the Plateau is ~5% (Fig. 9).

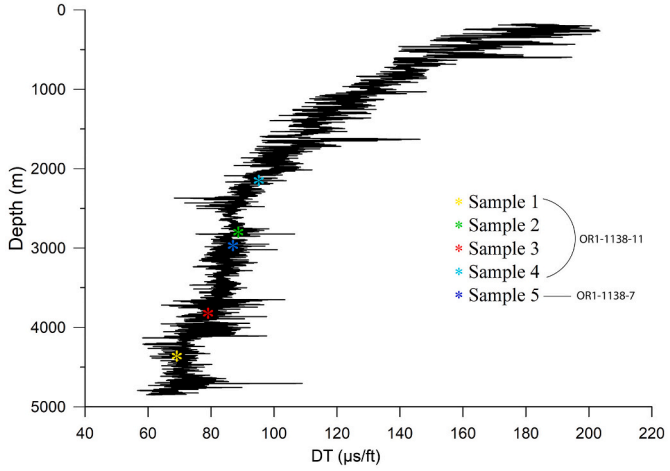

Fig. 8. A plot of 5 measurements on slowness (or sonic velocity) measured from rock samples superimposing on depth/slowness plot for FJ-1 well from Lin et al. (2003). The samples are recovered from sites OR1–1138-7 and OR1–1138-11 on the Kenting Plateau. See Fig. 2 for site locations.

4.3. Chronology and sedimentation rates

The chronology and the sedimentation rates of the core MD97–2145 were calculated from the ^{14}C dates. The age-depth curve shows that sediments below 1470 cm were deposited at much higher rates than the other intervals (Fig. 10a). The sedimentation rate below 1470 cm is approximately 247 cm/kyr, the highest rate showing in the core, followed by 141 cm/kyr between 1130 and 1470 cm. The lowest sedimentation rate is exhibited by the sediment layer between 900 and 1130 cm, around 40 cm/kyr. The sediment above 600 cm is deposited at an approximate rate of 90 cm/kyr (Fig. 10).

4.4. Measured oceanic currents

The VM-ADCP data collected during the oceanographic cruise OR2–2330 shows that the current velocity ranges from 0.3 m/s to 1.8 m/s on the Plateau (Fig. 11). The Kuroshio Knoll is the most elevated area, and it lies at ~70 m below the sea level in the Plateau. The highest current speed of 1.8 m/s has been observed above the Kuroshio Knoll between 40 and 55 m water depth, and it further decreases down to 1.6 cm/s near the seafloor (Fig. 11). The Kuroshio Current reaches the maximum speed when it hits the Knoll, and it gradually follows the Knoll topography. The southern part of the Kenting Plateau is more affected by strong currents than the Plateau's northern part (Fig. 11).

5. Discussion

The geomorphological interpretation of the seafloor is based on the multibeam bathymetry (with associated spatial derivatives) and seismic reflection data. The multibeam data reveal the evidence of a flat-topped surface in the Kuroshio Knoll, which signifies the extensive submarine erosion regime, and Kenting Basin, Hobi Basin, Nanwan Basin as sites of deposition. The erosive channels signify the effective medium for the sediment transport and dispersal to the respective basins. We interpret that the predominant mechanisms that control sediment erosion, transport, and deposition vary throughout the Plateau. The Kuroshio Knoll experiences the largest bottom shear stress related to the Kuroshio Current because it is located higher than the rest of the Plateau (Fig. 7).

5.1. Oceanic circulation around the Plateau

A bottom-current speed above 30 cm/s was measured in the northern South China Sea shelves (Wu, 2013), reaching a maximum speed of 80 cm/s (Qiu and Fang, 1999). In the present study, the observed bottom currents in the Kenting Plateau, especially in the Kuroshio Knoll, are

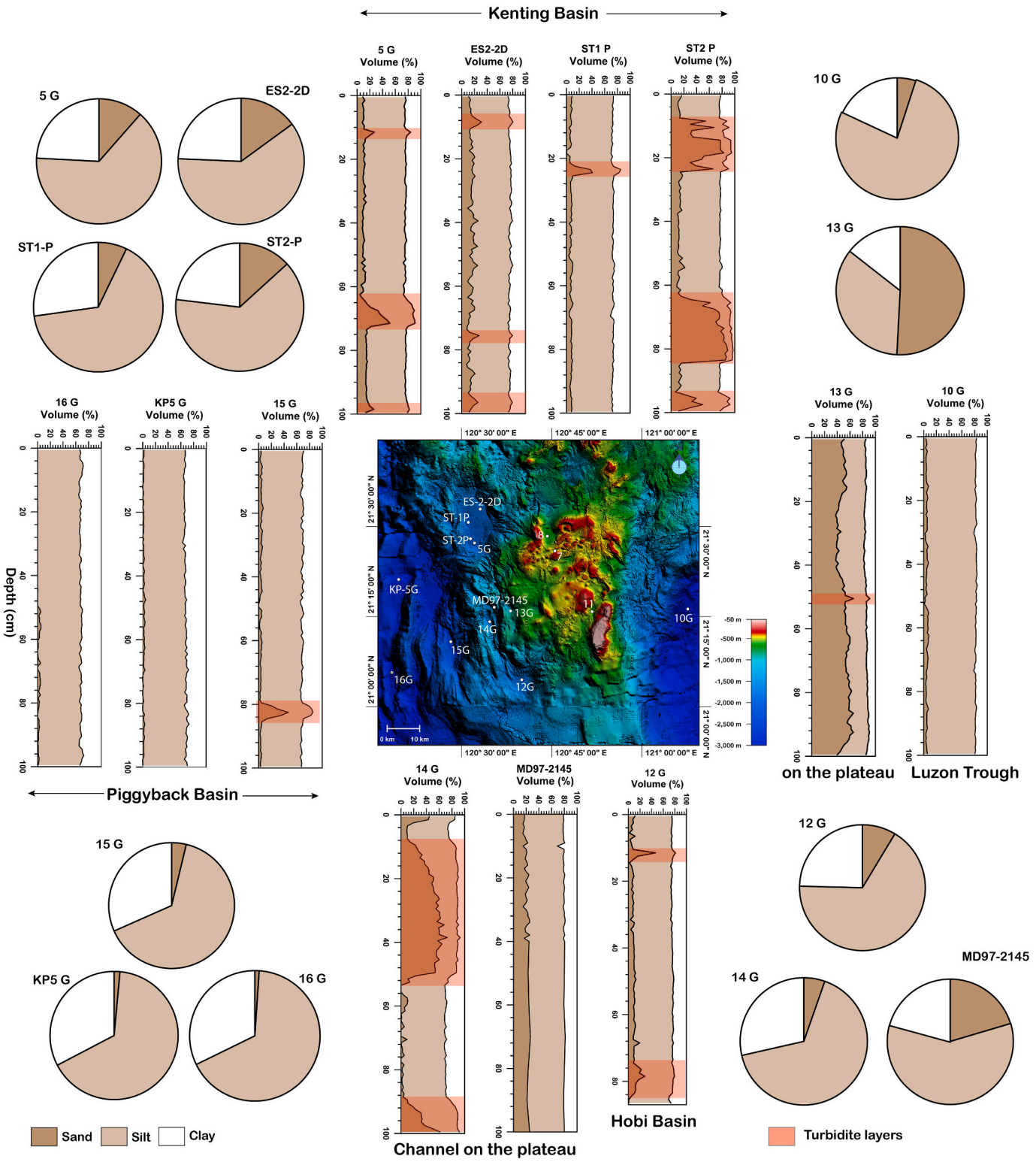

Fig. 9. Percentage of clay, silt and sand in different sediment cores collected from the Plateau and from the surrounding piggyback basins, and bathymetric map showing the location of the cores. The trend of the grain size showing a decreasing order away from the Plateau.

much higher, reaching 1.8 m/s on the surface water column (Fig. 11). The change in topography around the Plateau, from a deep trough (North Luzon trough) ~3500 m to a sudden rise of ~500 m or less water depth with an average slope of more than 10°, dramatically affects the velocity and impact of the Kuroshio Current to the Plateau. Before entering the South China Sea, when the Kuroshio Current encounters the topographic high of the Kenting Plateau, it squeezes in its thickness, and its velocity strengthens as a result of Bernoulli's effect on the top of Kenting Plateau, reaching maximum speeds of 1.8 m/s, which further intensifies erosion on the seafloor. Bernoulli's effect is basically the increase in the speed of the fluid with the decrease in static pressure. From the VM-ADCP data collected during cruise OR2–2330, it has been found that the strength of Kuroshio Current around the Plateau ranges from ~50 cm/s around the deeper plateau surface to as high as 1.8 m/s on the

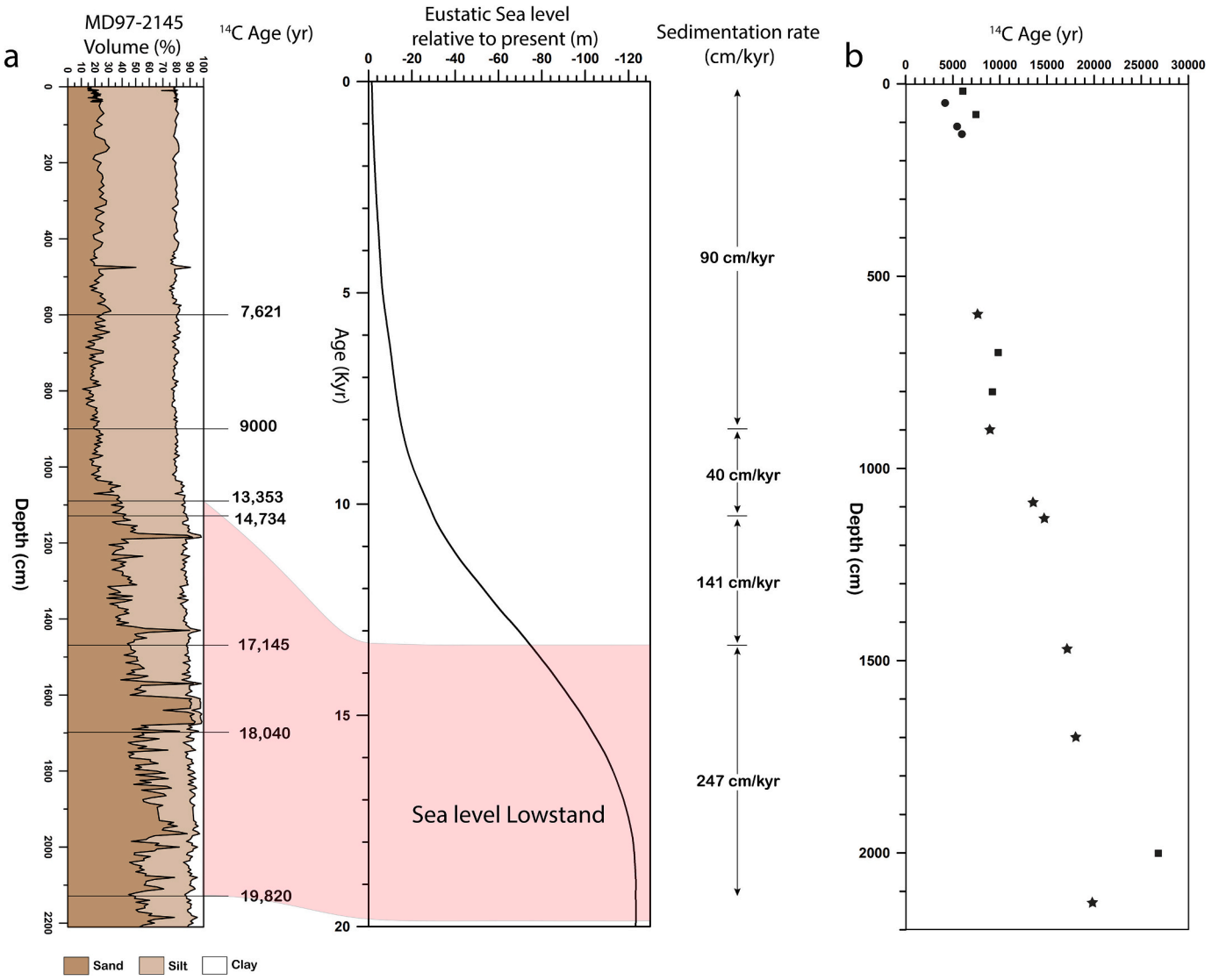

Fig. 10. a) Volume percentage distribution of clay, silt and sand of the core MD 972145. The respective ^{14}C ages are labeled near the core. The ^{14}C dates corelated with the global eustatic sea level relative to present from Bintanja et al., 2005. The transparent red layer shows the higher sedimentation rate in the sea level lowstand. b) Age-depth plot of the core MD 972145. ^{14}C ages for 0.2, 0.8, 7, 8, and 20 m (closed squares) are not in the right order of succession and are older than the age of the next deeper sample. The ^{14}C ages for 0.5, 1.1, and 1.3 m (filled circles) are in the right order of succession but they may also not be reliable because those samples were taken from an interval characterized by vertical sediment mixing. Dates from other samples (filled star) do follow a normal age-depth relation (i.e., age increase with depth). (For interpretation of the references to colour in this figure legend, the reader is referred to the web version of this article.)

top of Kuroshio Knoll (Fig. 11), which is probably sufficient to erode the seafloor and prevent from sediment deposition on the top of the Plateau. The irregular flat-topped topography of the Knoll is thus probably shaped by the Kuroshio Current. The substantial current velocity on the top of the Plateau surface could generate erosion, sand/gravel transportation, and the observed dune field in the Nanwan Basin (Fig. 6).

Internal gravity waves are propagating disturbances of the ocean's density stratification set up primarily by wind and tides. These waves resemble surface gravity waves but with buoyancy rather than gravity, which gives their reestablishing power, consequently travel many kilometers from their sources before breaking (Ray and Mitchum, 1996). These waves can cause strong seafloor sediment resuspension and produce nepheloid layers for sediment transportation in both deep and shallow-water environments. The largest internal waves in the Luzon Strait emerge due to the double ridge structure in the northern section of Luzon Strait, which creates a 100 km scale resonant cavity for the ~100 km wavelength semi-diurnal internal tide (Buijsman et al., 2014). While transiting, the tidal flow results in vertical displacements of the ocean layers that reach up to 500 m, with static instabilities >200 m high and exceed the associated depth-integrated turbulent dissipation levels by a factor of 1000–10,000 of the open ocean values (Pinkel et al., 2012; Alford et al., 2015), which may result in the erosion of the Plateau. These internal tides are significantly affected by the strong Kuroshio Current, steepen into sharp wave fronts and eventually break on the continental shelf resulting in seafloor erosion and sediment resuspension along the path of the internal waves (Alford et al., 2015) as seen in the northeastern slope of the South China Sea (Jia et al., 2019). Similar sediment erosion and bedform creation has also been found in Mozambican continental margin due to internal waves (Miramontes et al., 2020). The Kenting Plateau could be thus affected by internal waves, which could also contribute towards its erosion and sediment transportation/removal.

5.2. *Submarine erosion and deposition model*

A previous study showed that the upper accretionary prism, Kenting

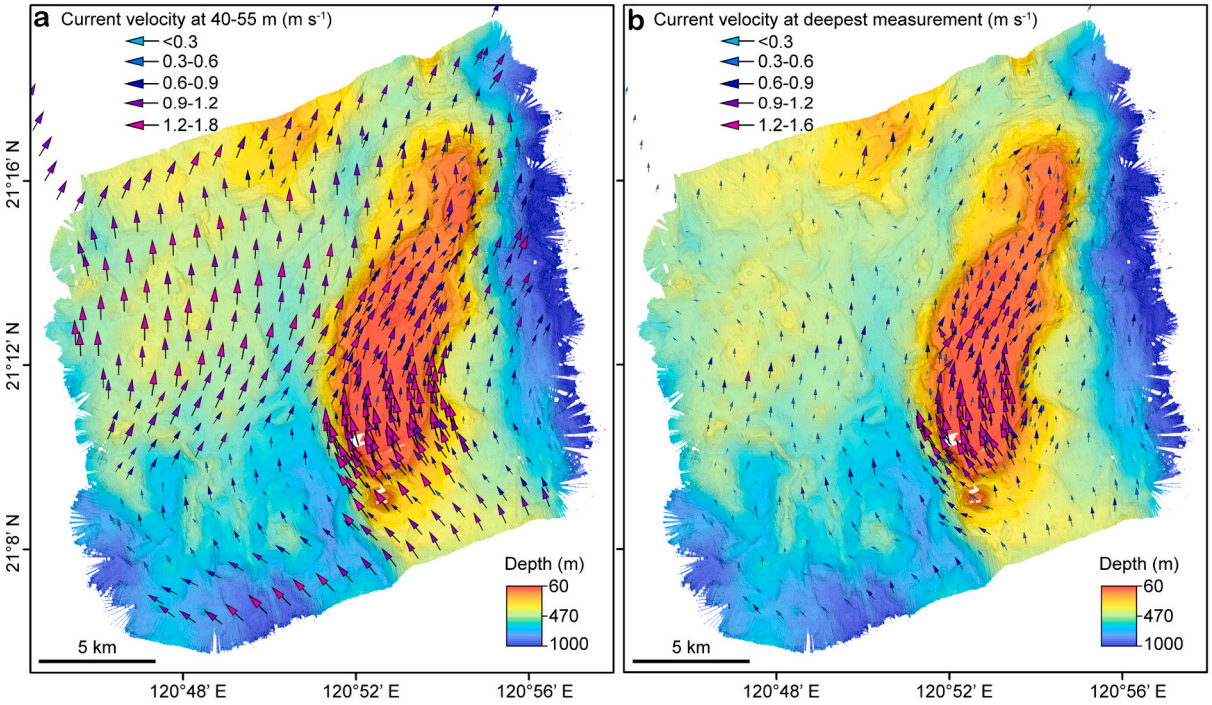

Fig. 11. Current velocity from VM-ADCP acquired during OR2–2330 cruise conducted during 9/18/2018–9/22/2018, (a) averaged between 40 m and 55 m water depth; and (b) at deepest measurements (near the seafloor and at around 60–70 m on the Kuroshio Knoll and at about 200 m water depth in the rest of the area).

Plateau, is covered with a very thin layer of Quaternary sediments (Damuth, 1980). This agrees with our observations and implies that the deposition in this area is limited only to some part of the Plateau, mostly to the basins and small depressions present in the Plateau, and erosional processes or non-deposition processes dominate especially in the eastern flank of the Plateau. Erosion appears to dominate on the Plateau, and further helps in exuviating the sediment away from the Plateau through different processes. It is evident from the substantial current velocity of ~1.2 m/s near the surface of the Kuroshio Knoll that the Kuroshio Current erodes the Plateau surface, winnows the loose particles away from the Plateau, which is finally deposited in the farther basins and leaves the remaining coarser materials in the Plateau (Figs. 5, 6, 12). The seafloor connecting the Plateau to different basins in and around the Plateau is characterized by irregular seafloor, with the presence of channels, suggesting that gravity-driven processes may also play an essential role in transporting sediment from the top of the Plateau through channels or gullies to the deep basin floor. For instance, the Kenting Basin in the NW part is connected with the Plateau through several erosive gullies (Figs. 2, 3b). These erosive channels are the pathway for the coarse sediments from the Plateau to be deposited in the largest basin in that area as turbidite deposits (Figs. 4a, 9). The Nanwan Basin is located in the northern part of the Plateau in between two structural highs with a water depth ranging from 550 m in the southern part of the basin to 900 m in the northern part of the basin with an average slope of 1.4 ^{o} to 3 ^{o}. The asymmetry of the dunes observed in the Nanwan Basin suggests a northward migration, and thus the bottom currents that formed these flowed in the same direction. Such bedforms, which are predominantly sandwaves or dunes, are seen and recognized in the deep water around several places and indicate bottom current processes (Bøe et al., 2015; Ma et al., 2016; Miramontes et al., 2019b).

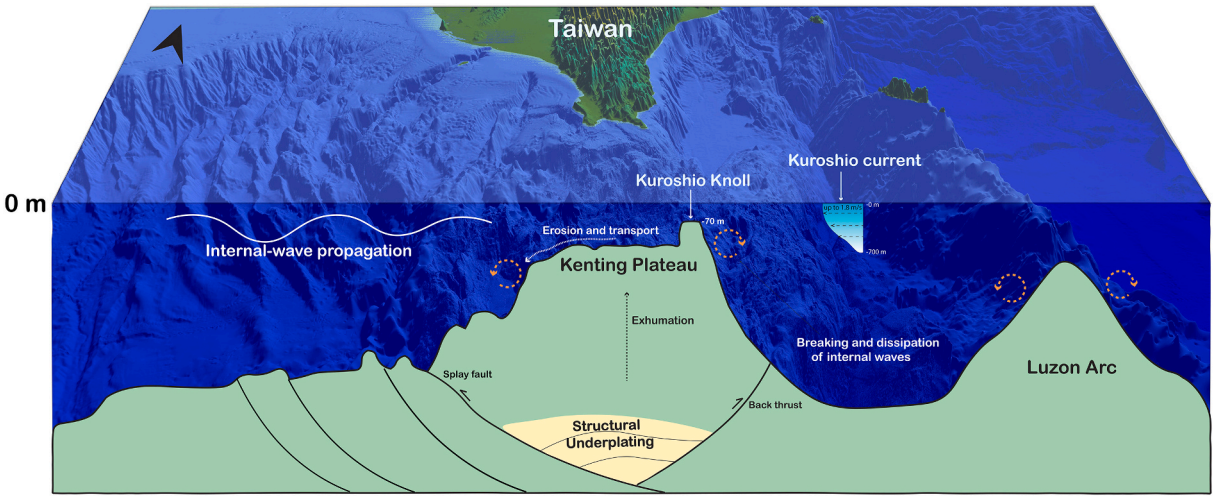

Fig. 12. Schematic representation of the processes controlling sediment erosion and transport on the Kenting Plateau.

The slope changes from ~6 ° – 10 ° in the southern part of the Nanwan Basin to ~1.5 ° in the basin's northern part. The decrease in slope is indicative of a change in flow regime, from an erosive regime in the southern part to a depositional regime in the northern part (Fig. 7). The bedforms' orientation agrees with the current direction observed in the ADCP data (Fig. 11). The bedforms are composed of fine sands to coarse sands, and fragments of shells and benthic organisms (Fig. 6), suggesting a high-energy sediment transport regime. Due to their high surface to weight ratio, shell fragments are easily carried away by the currents with the sediments through traction.

The sediment core analysis from different basins helps to understand the sediment distribution pattern around the Plateau. The eroded sediments from the Plateau have been transferred to deep basins around the Plateau. From the grain size analysis, the cores are composed of mostly hemipelagic sediments with few patches of turbidite layers in between, which are characterized by fining-upward units (from coarse sand to fine silt and clay). The core 13G located on the Plateau shows the highest percentage of sand ~51%, with the minimum amount of clay ~ <15%. The top 100 cm of the core MD 97–2145 located on the elevated ridge of a submarine channel in the Plateau show ~20% sand content. In contrast, the cores located in Kenting Basin (5G, STP1, STP2, ES2–2-D) consist of mostly mud with clay percentages of more than 20% and ~ 8 to 15% of sand. The cores (KP5-G, 15G, 16G) in the slope basins located west to the Plateau show negligible sand content ~1 to 3.5% with ~40% of clay content. The core 12G in the Hobi Basin show similar results as Kenting Basin cores with ~8.65% of sand content. Moreover, the core 10G in the Luzon trough consists of mostly mud with about 5% of sand content (Fig. 9). From the sand contents, it is clear that the core located on the Plateau exhibit the most percentage of sand content in the core; as we move away from the Plateau to different basins around the Plateau, the sand content started to decrease with an increase in mud content. The Plateau serves as a source for the sediment in this region, particularly to the basins surrounded by it. The strong Kuroshio Current not only exuviates the Plateau leading to further erosion of the bedrock, but also helps to distribute the sediments to the surrounding basins.

From the multibeam bathymetric data and seismic reflection data, we have identified different domains: depositional basins, truncated basins, and erosional surfaces or bed outcrops. The grab samples collected around the Plateau are gravels (sandstone, siltstone, mudstone, carbonate rock), coarse sand, and silt with abundant shell fragments (Fig. 5c). The site OR1–1138-11 lies NW of the Kuroshio Knoll in a small depression at around 600 m water depth. Those gravels must be derived from local bathymetric high, the Kuroshio Knoll, as slope failure. They cannot originate from Taiwan Island as the Plateau is surrounded by bathymetric lows (Fig. 1), and gravels of few centimeters in diameter cannot be transported in suspension. The Kuroshio Knoll, the nearest local high platform to those gravels, shows few concave slopes up to ~40°, which correspond to submarine landslide scars (Fig. 7). The gravels are sub-rounded to rounded (Fig. 5a), and the shape of the gravels could be interpreted as the result of transport and abrasion. They were thus probably transported and abraded by currents for long periods. The bathymetric profiles across the gravel location (A-A′ and B-B′ in Fig. 7b) shows that the gravels lie in a depression in the north-west base of the Knoll and the possible source of the gravel is from Kuroshio Knoll through mass wasting or slope failure (Fig. 7). We suggest that the transport and abrasion of gravels could have occurred on the subaerial Kuroshio Knoll during sea-level lowstand, probably during the Last Glacial Maximum (LGM) when the sea level was −120 m lower than the present day (Wang and Wang, 1990; Lambeck and Chappell, 2001) and the Kuroshio Knoll was exposed as an island ~50 m above the sea level. The gravels might have been transported from the Kuroshio Knoll by sediment gravity flows or slope failures and eventually found its place from where it was recovered. By contrast, gravels recovered at site OR1–1138-7 (420 m deep) are angular in shape (Fig. 5b). We interpret the angular feature to result from slope failure with less transportation and abrasion by currents and waves. The surrounding shallowest bathymetry around this site is ~300 m deep, indicating there were no emerged areas even during the sea-level lowstand. Gravels at site OR1–1138-7 are interpreted as lag deposits, flooring the hard-erosive surface.

All the recovered gravels indicate that the parent rocks are well-cemented and lithified. The parent rocks originate from nearby bathymetric highs, defined from reflection seismic data as "hard surface" and underlain by basement rocks (Fig. 4b). The basement rocks must have been buried in a certain depth to achieve the state of diagenesis as observed from the recovered gravels. The gravels show high P-wave velocity up to 3.45 km/s. After comparing these velocities with that of a nearby borehole FJ-1 in Tainan Basin (Lin et al., 2003), we found that the parent rocks would have been buried in a depth ranging 2 to 4 km below seafloor. That indicates the seafloor would have to erode and uncover the surface sediments at least 2 km to get the gravel's parent rocks.

5.3. Morphological evolution of Kuroshio Knoll

The South China Sea was more or less semi-enclosed during MIS 3–5 when the sea level was −75 m to −70 m and − 55 m, respectively (Lambeck and Chappell, 2001). During the LGM, the size and configuration of the South China Sea were significantly reduced. During that time, the sea level in the South China Sea was 100–120 m below the present sea level and transformed it into a semi-enclosed gulf, which was connected to the Pacific Ocean only through the north-eastern part of the South China Sea through Bashi Channel (Wang and Wang, 1990; Lambeck and Chappell, 2001). Therefore, during that time, the surface circulation pattern was probably different from that of today (Wang et al., 1995). Sea-level variations may play a significant role on the intrusions of Kuroshio Current in the South China Sea. From our bathymetric data, it is evident that the Kuroshio Knoll has emerged above the sea surface during the last glacial period. It could have probably reached a height of 50 to 60 m above sea level during LGM as the present height of the Plateau is ~70 m below sea level.

Based on AMS ^{14}C dates, the sediments below the depth 1460 cm of MD97–2145 core was deposited during the LGM when sea level was approximately 120 m lower than the present and the sedimentation rate during this period was at its maximum around 247 cm/kyr (Fig. 10a). Sediments below 1100 cm contain mostly sands with less amount of silts and clay. A few turbidite layers with a basal foraminiferal sand layer (> 60% of sand) of a few cm in thickness and an overlying finer silty sand layer were also present in the core. These turbidite layers are interpreted as slope failure or mass wasting deposits from the Plateau. The lowest sedimentation rate recorded in the core between 900 cm and 1160 cm is 40 cm/kyr. The significant decrease in the sedimentation rate maybe during Termination I when the sea level started to rise. The sedimentation rate in the top 600 cm of the core shows around 90 cm/kyr which might be due to the rise in sea level. After correlating to the global eustatic sea level curve (Bintanja et al., 2005) it was found that the sedimentation rate is higher during sea level lowstand compared to the deglacial period. The sediment is mainly composed of sand layers during the glacial period suggesting deposit of slope failure of mass wasting. The higher sedimentation rate during LGM suggests that the Kuroshio Current might be more effective on the Plateau surface due to lowered eustatic sea level. The Plateau could have been intensely eroded by Kuroshio Current and internal waves, tides, and mass wasting during the glacial period. Long-term erosion on the Plateau by various agents, specifically by Kuroshio Current, removes much mass from the Plateau.

At site OR1–1138-11-1 on top of the Kuroshio Knoll (63 m deep), living green algae (*Halimeda sp.*) and other organisms along with carbonate debris were sampled by sediment grab (Fig. 5d), suggesting that the flat-topped surface of Kuroshio Knoll is composed of hard, well-lithified rocks. Several gravels of siliciclastic and carbonate rocks found at site OR-1-1138-11 near the Kuroshio Knoll also indicate that the Kuroshio Knoll is underlain by hard substrate. Concave slopes in

well-lithified rock settings are usual as they are more prone to build steeper slopes than siliciclastic-sediment settings (e.g., Adams et al., 2013). The top of the Kuroshio Knoll is thus floored by hard bedrocks.

Crustal structure analysis of the Manila accretionary wedge reveals structural underplating below the wedge (Doo et al., 2015; Eakin et al., 2013; Lester et al., 2013). The structural underplating, along with the compressional tectonics in the area, governs the uplift of the Plateau. In our study, we found that the extensive mass removal from the Plateau also helps in uplifting the Plateau. Uplift of the Plateau due to the isostatic rebound of the lithosphere may compensate the mass removal by erosion (e.g., Willett, 1999; Whipple and Meade, 2006; Korup and Schlunegger, 2009).

6. Conclusion

The Kenting Plateau is unusual shallow (400–700 m water depth) topographic low relief surfaces in the northern Manila accretionary prism with a dimension of 30 km × 40 km. In the SE domain of the Plateau, there is an elevated flat area, named "Kuroshio Knoll" in this study, located at water depths of 60–70 m with a dimension of 3 × 7 km.

Multibeam bathymetry and seismic reflection datasets plan the premise of our geomorphological understandings and interpretation of sedimentary processes on the Plateau. The multibeam data reveal significant erosion and deposition around the Plateau, which is fully supported by observing strong bottom currents in VM-ADCP data.

Current velocities observed from the ADCP data on the Plateau surface reach up to 1.6 m/s near the Kuroshio Knoll seafloor. These strong bottom currents are probably at the origin of the observed seafloor erosion and dune field. Bottom currents are the highest on the Kuroshio Knoll because this is the shallowest part of the Plateau, and it is thus more exposed to the Kuroshio Current.

Reflection seismic data and sediment cores show that most of the Plateau surface, especially in the eastern half, is an erosive surface underlain by well-lithified sedimentary rocks, with coarse-grained materials (e.g., gravels, sands, carbonate grains) accumulated in local depressions on the Plateau surface. The sand and silt contents of the cores collected in the basin seafloor around the Plateau show a decreasing trend in grain size away from the Plateau, suggesting that submarine erosion is effective, thereby accumulating coarser sediments on the Plateau and removing fine particles from the Plateau, which are deposited in distal regions.

Our data reveal that the Kenting Plateau has experienced substantial submarine erosion, with the amount of exhumation up to a few kilometers, increasing exhumation towards the rear wedge. We interpret that this intense erosion is due to Kuroshio Current and the uplift of the Kenting Plateau is partly due to isostatic rebound owing to sediment removal by erosion, by structural underplating below the wedge, and by other processes related to compressional tectonics in the accretionary wedge (e.g., splay faulting, structural underplating, and backthrusting).

CRediT authorship contribution statement

Prabodha Das: Formal analysis, Writing - original draft, Writing - review & editing. Andrew **Tien-Shun Lin:** Supervision, Conceptualization, Methodology, Funding acquisition. **Min-Pen Philip Chen:** Formal analysis. **Elda Miramontes:** Formal analysis. **Char-Shine Liu:** Formal analysis. **Neng-Wei Huang:** Formal analysis. **Jennifer Kung:** Resources. **Shu-Kun Hsu:** Formal analysis. **Radha Krishna Pillutla:** Formal analysis. **Kalyani Nayak:** Formal analysis.

Declaration of Competing Interest

The authors declare that they have no known competing financial interests or personal relationships that could have appeared to influence the work reported in this paper.

Acknowledgement

This research was funded by the Ministry of Science and Technology, Taiwan, through grants MOST108-2116-M-008-002 and MOST109-2611-M-008-001. Valuable reviews by Tim Byrne and Shaoru Yin are greatly appreciated and their comments have significantly improved the paper.

References

Adams, E.W., Kenter, J.A., Verwer, K., Playton, T.E., Harris, P.M., 2013. So different, yet so similar: comparing and contrasting siliciclastic and carbonate slopes. Deposits, architecture, and controls of carbonate margin, slope, and basinal settings. SEPM Spec. Publ. 105, 14–25.

Alford, M.H., Peacock, T., MacKinnon, J.A., Nash, J.D., Buijsman, M.C., Centurioni, L.R., Chao, S.Y., Chang, M.H., Farmer, D.M., Fringer, O.B., Fu, K.H., 2015. The formation and fate of internal waves in the South China Sea. Nature 521 (7550), 65–69.

Audet, D.M., 1995. Modelling of porosity evolution and mechanical compaction of calcareous sediments. Sedimentology 42, 355–373.

Audet, D.M., 1996. Compaction and overpressuring in Pleistocene sediments on the Louisiana Shelf, Gulf of Mexico. Mar. Pet. Geol. 13, 467–474.

Bintanja, R., Van De Wal, R.S.W., Oerlemans, J., 2005. Modelled atmospheric temperatures and global sea levels over the past million years. Nature 437 (7055), 125–128.

Blott, S.J., Pye, K., 2001. GRADISTAT: a grain size distribution and statistics package for the analysis of unconsolidated sediments. Earth Surf. Process. Landf. 26 (11), 1237–1248.

Bøe, R., Skarðhamar, J., Rise, L., Dolan, M.F., Bellec, V.K., Winsborrow, M., Skagseth, Ø., Knies, J., King, E.L., Walderhaug, O., Chand, S., 2015. Sandwaves and sand transport on the Barents Sea continental slope offshore northern Norway. Mar. Pet. Geol. 60, 34–53.

Buijsman, M.C., Klymak, J.M., Legg, S., Alford, M.H., Farmer, D., MacKinnon, J.A., Nash, J.D., Park, J.H., Pickering, A., Simmons, H., 2014. Three-dimensional double-ridge internal tide resonance in Luzon Strait. J. Phys. Oceanogr. 44 (3), 850–869.

Centurioni, L.R., Niiler, P.P., Lee, D.K., 2004. Observations of inflow of Philippine Sea surface water into the South China Sea through the Luzon Strait. J. Phys. Oceanogr. 34 (1), 113–121.

Chern, C.S., Wang, J., 1998. A numerical study of the summertime flow around the Luzon Strait. J. Oceanogr. 54 (1), 53–64.

Damuth, J.E., 1980. Quaternary sedimentation processes in the South China Basin as revealed by echo-character mapping and piston-core studies. The tectonic and geologic evolution of southeast Asian seas and islands. Am. Geophys. Union Geophys. Monogr. 23, 105–125.

Dirgantara, F., Chiang, H.T., Lin, A.T., Liu, C.S., Chen, S.C., 2020. Depositional influence of submarine channel migration on thermal properties of the lower Fangliao Basin, offshore southwestern Taiwan. Mar. Geophys. Res. 41 (1), 1–23.

Doo, W.B., Lo, C.L., Kuo-Chen, H., Brown, D., Hsu, S.K., 2015. Exhumation of serpentinized peridotite in the northern Manila subduction zone inferred from forward gravity modeling. Geophys. Res. Lett. 42 (19), 7977–7982.

Eakin, D.H., McIntosh, K.D., Van Avendonk, H.J.A., Lavier, L., Lester, R., Liu, C.S., Lee, C. S., 2013. Crustal-scale seismic profiles across the Manila subduction zone: the transition from intra oceanic subduction to incipient collision. J. Geophys. Res. Solid Earth 119 (1), 1–17.

Fener, M., 2011. The effect of rock sample dimension on the P-wave velocity. J. Nondestruct. Eval. 30 (2), 99–105.

García, M., Hernández-Molina, F.J., Alonso, B., Vázquez, J.T., Ercilla, G., Llave, E., Casas, D., 2016. Erosive sub-circular depressions on the Guadalquivir Bank (Gulf of Cadiz): Interaction between bottom current, mass-wasting and tectonic processes. Mar. Geol. 378, 5–19.

Hernández-Molina, F.J., Campbell, S., Badalini, G., Thompson, P., Walker, R., Soto, M., Conti, B., Preu, B., Thieblemont, A., Hyslop, L., Miramontes, E., Morales, E., 2017. Large bedforms on contourite terraces: sedimentary and conceptual implications. Geology 46, 27–30.

Huang, C.H., 2002. A Study of Sea Surface Temperature since the Last Glacial Period in the Bashi Strait from the MD972145 Core. MS Thesis. Institute of Oceanography, National Taiwan University, Taiwan (in Chinese).

Issler, D.R., 1992. A new approach to shale compaction and stratigraphic restoration, Beaufort-Mackenzie Basin and Mackenzie Corridor, northern Canada. AAPGBull. 76, 1170–1189.

Jan, S., Yang, Y.J., Wang, J., Mensah, V., Kuo, T.H., Chiou, M.D., Chern, C.S., Chang, M. H., Chien, H., 2015. Large variability of the Kuroshio at 23.75 N east of Taiwan. J. Geophys. Res. Oceans 120 (3), 1825–1840.

Jia, Y., Tian, Z., Shi, X., Liu, J.P., Chen, J., Liu, X., Ye, R., Ren, Z., Tian, J., 2019. Deep-sea sediment resuspension by internal solitary waves in the northern South China Sea. Sci. Rep. 9 (1), 1–8.

Jiang, H., Björck, S., Ran, L., Huang, Y., Li, J., 2006. Impact of the Kuroshio current on the South China Sea based on a 115,000 year diatom record. J. Quatern. Sci. Publ. Quatern. Res. Assoc. 21 (4), 377–385.

Korup, O., Schlunegger, F., 2009. Rock-type control on erosion-induced uplift, eastern Swiss Alps. Earth Planet. Sci. Lett. 278 (3–4), 278–285.

Lambeck, K., Chappell, J., 2001. Sea level change through the last glacial cycle. Science 292 (5517), 679–686.

Lester, R., McIntosh, K., Van Avendonk, H.J., Lavier, L., Liu, C.S., Wang, T.K., 2013. Crustal accretion in the Manila trench accretionary wedge at the transition from subduction to mountain-building in Taiwan. Earth Planet. Sci. Lett. 375, 430–440.
Li, L., Nowlin Jr., W.D., Jilan, S., 1998. Anticyclonic rings from the Kuroshio in the South China Sea. Deep-Sea Res. I Oceanogr. Res. Pap. 45 (9), 1469–1482.
Lin, A.T., Watts, A.B., Hesselbo, S.P., 2003. Cenozoic stratigraphy and subsidence history of the South China Sea margin in the Taiwan region. Basin Res. 15, 453–478.
Li, L., Wu, B.Y., 1989. A Kuroshio loop in South China Sea?—on circulations of the north-eastern South China Sea. J Oceanogr Taiwan Strait 8(1), 89–95.
Liang, W.D., Yang, Y.J., Tang, T.Y., Chuang, W.S., 2008. Kuroshio in the Luzon Strait. Journal of Geophysical Research: Oceans 113(C8).
Lin, A.T., Liu, C.S., Lin, C.C., Schnurle, P., Chen, G.Y., Liao, W.Z., Chuang, H.R., Teng, L. S., Wu, M.S., 2008. Tectonic features associated with the overriding of an accretionary wedge on top of a rifted continental margin: an example from Taiwan. Mar. Geol. 255, 186–203.
Lin, A.T., Yao, B., Hsu, S.K., Liu, C.S., Huang, C.Y., 2009. Tectonic features of the incipient arc-continent collision zone of Taiwan: Implications for seismicity. Tectonophysics 479 (1–2), 28–42.
Liu, C.S., Lundberg, N., Reed, D.L., 1992. Gravity and magnetics studies off southwestern Taiwan and their tectonic implication. EOS Trans. AGU 73, 558.
Ma, X., Yan, J., Hou, Y., Lin, F., Zheng, X., 2016. Footprints of obliquely incident internal solitary waves and internal tides near the shelf break in the northern South China Sea. J. Geophys. Res. Oceans 121 (12), 8706–8719.
Miramontes, E., Penven, P., Fierens, R., Droz, L., Toucanne, S., Jorry, S.J., Jouet, G., Pastor, L., Jacinto, R.S., Gaillot, A., Giraudeau, J., 2019a. The influence of bottom currents on the Zambezi Valley morphology (Mozambique Channel, SW Indian Ocean): in situ current observations and hydrodynamic modelling. Mar. Geol. 410, 42–55.
Miramontes, E., Jorry, S.J., Jouet, G., Counts, J.W., Courgeon, S., Le Roy, P., Guerin, C., Hernández-Molina, F.J., 2019b. Deep-water dunes on drowned isolated carbonate terraces (Mozambique Channel, south-West Indian Ocean). Sedimentology 66 (4), 1222–1242.
Miramontes, E., Jouet, G., Thereau, E., Bruno, M., Penven, P., Guerin, C., Le Roy, P., Droz, L., Jorry, S.J., Hernández-Molina, F.J., Thiéblemont, A., 2020. The impact of internal waves on upper continental slopes: insights from the Mozambican margin (Southwest Indian Ocean). Earth Surf. Process. Landf. 45 (6), 1469–1482.
Mitchell, N.C., 2014. Bedrock erosion by sedimentary flows in submarine canyons. Geosphere 10 (5), 892–904.
Mitchell, N.C., Dade, W.B., Masson, D.G., 2003. Erosion of the submarine flanks of the Canary Islands. J. Geophys. Res. Earth Surf. 108 (F1), 3-1-3-11.
Montgomery, D.R., Greenberg, H.M., 2000. Local relief and the height of Mount Olympus. Earth surface processes and landforms. J. Br. Geomorphol. Res. Group 25 (4), 385–396.
Nan, F., He, Z., Zhou, H., Wang, D., 2011. Three long-lived anticyclonic eddies in the northern South China Sea. J. Geophys. Res. Oceans 116 (C5), 879–889.
Nan, F., Xue, H., Yu, F., 2015. Kuroshio intrusion into the South China Sea: a review. Prog. Oceanogr. 137, 314–333.
Nitani, H., 1972. Beginning of the Kuroshio. In: Stommel, H., Yashida, K. (Eds.), Kuroshio: Physical Aspects of the Japan Current. University of Washington Press, pp. 129–163.
Pinkel, R., Buijsman, M., Klymak, J.M., 2012. Breaking topographic lee waves in a tidal channel in Luzon Strait. Oceanography 25 (2), 160–165.
Qiu, D.Z., 1984. A west-flowing current in the northern part of the South China Sea in summer. Trop. Oceanol. 3, 65–73.
Qiu, Z., Fang, W.D., 1999. Vertical variation of spring sea current in Northern South China Sea. Tropical Oceanogr 18, 32–39.
Qiu, B., Lukas, R., 1996. Seasonal and interannual variability of the North Equatorial Current, the Mindanao Current, and the Kuroshio along the Pacific western boundary. Journal of Geophysical Research: Oceans 101 (C5), 12315–12330.
Qu, T., Lukas, R., 2003. The bifurcation of the North Equatorial current in the Pacific. J. Phys. Oceanogr. 33 (1), 5–18.
Ray, R.D., Mitchum, G.T., 1996. Surface manifestation of internal tides generated near Hawaii. Geophys. Res. Lett. 23 (16), 2101–2104.
Rebesco, M., Hernández-Molina, F.J., Van Rooij, D., Wåhlin, A., 2014. Contourites and associated sediments controlled by deep-water circulation processes: state-of-the-art and future considerations. Mar. Geol. 352, 111–154.
Reed, D.L., Lundberg, N., Liu, C.-S., Kuo, B.-Y., 1992. Structural relations along the margins of the offshore Taiwan accretionary wedge: implications for accretion and crustal kinematics. Acta Geol. Taiwan. 30, 105–122.
Romagnoli, C., Casalbore, D., Chiocci, F.L., 2012. La Fossa Caldera breaching and submarine erosion (Vulcano island, Italy). Mar. Geol. 303, 87–98.
Shaw, P.T., 1991. The seasonal variation of the intrusion of the Philippine Sea water into the South China Sea. J. Geophys. Res. Oceans 96 (C1), 821–827.
Wang, L., Wang, P., 1990. Late Quaternary paleoceanography of the South China Sea: Glacial-interglacial contrasts in an enclosed basin. Paleoceanography 5 (1), 77–90.
Wang, P., Shaw, L., Bian, Y., Jian, Z., 1995. Late Quaternary paleoceanography of the South China Sea: surface circulation and carbonate cycles. Mar. Geol. 127 (1–4), 145–165.
Watson, S.J., Whittaker, J.M., Lucieer, V., Coffin, M.F., Lamarche, G., 2017. Erosional and depositional processes on the submarine flanks of Ontong Java and Nukumanu atolls, western equatorial Pacific Ocean. Mar. Geol. 392, 122–139.
Whipple, K.X., Meade, B.J., 2006. Orogen response to changes in climatic and tectonic forcing. Earth Planet. Sci. Lett. 243 (1–2), 218–228.
Willett, S.D., 1999. Orogeny and orography: the effects of erosion on the structure of mountain belts. J. Geophys. Res. Solid Earth 104 (B12), 28957–28981.
Wu, C.R., 2013. Interannual modulation of the Pacific Decadal Oscillation (PDO) on the low-latitude western North Pacific. Prog. Oceanogr. 110, 49–58.
Wu, C.R., Chiang, T.L., 2007. Mesoscale eddies in the northern South China Sea. Deep Sea Research Part II: Topical Studies in Oceanography 54(14-15), 1575–1588.
Wyrtki, K., 1961. Scientific results of marine investigations of the South China Sea and the Gulf of Thailand 1959–1961 physical oceanography of the Southeast Asian Waters. NAGA Report 2, 195.
Xiu, P., Chai, F., Shi, L., Xue, H., Chao, Y., 2010. A census of eddy activities in the South China Sea during, 1993–2007. J. Geophys. Res. 115 (C03012), 1–15.
Zhai, F., Hu, D., 2013. Revisit the interannual variability of the North Equatorial current transport with ECMWF ORA-S3. J. Geophys. Res. Oceans 118 (3), 1349–1366.
Zhao, Z., Mitchell, N.C., Quartau, R., Tempera, F., Bricheno, L., 2019. Submarine platform development by erosion of a Surtseyan cone at Capelinhos, Faial Island, Azores. Earth Surf. Process. Landf. 44 (15), 2982–3006.